CHALMERS
UNIVERSITY OF TECHNOLOGY

Field exposure of FeCrAl model alloys in a waste-fired boiler at 600°C: The influence of Cr and Si on the corrosion behaviour

Downloaded from: https://research.chalmers.se, 2024-07-27 04:21 UTC

Citation for the original published paper (version of record):
Eklund, J., Olausson, M., Jonsson, B. et al (2019). Field exposure of FeCrAl model alloys in a waste-fired boiler at 600°C: The influence of Cr and
Si on the corrosion behaviour. Materials and Corrosion, 70(8): 1476-1485.
http://dx.doi.org/10.1002/maco.201810618

N.B. When citing this work, cite the original published paper.

research.chalmers.se offers the possibility of retrieving research publications produced at Chalmers University of Technology.
It covers all kind of research output: articles, dissertations, conference papers, reports etc. since 2004.
research.chalmers.se is administrated and maintained by Chalmers Library

(article starts on next page)

Check for updates

Received: 23 October 2018 | Revised: 11 February 2019 | Accepted: 24 February 2019

DOI: 10.1002/maco.201810618

ARTICLE

Materials and Corrosion

Field exposure of FeCrAl model alloys in a waste-fired boiler at 600°C: The influence of Cr and Si on the corrosion behaviour

Johan Eklund[1] | Maria Dolores Paz[1] | Bo Jönsson[2] | Jesper Liske[1] | Jan-Erik Svensson[1] | Torbjörn Jonsson[1]

[1]Department of Chemistry and Chemical Engineering, Division of Energy and Materials, Chalmers University of Technology, Gothenburg, Sweden

[2]Department of Research and Development, Kanthal AB, Hallstahammar, Sweden

Correspondence
Johan Eklund, Department of Chemistry and Chemical Engineering, Division of Energy and Materials, Chalmers University of Technology, 41296 Gothenburg, Sweden.
Email: johekl@chalmers.se

Abstract

The aim of this study was to examine the performance of FeCrAl model alloys in a waste-fired boiler and investigate the influence of chromium and silicon content on the corrosion behaviour. The investigation was executed by utilising an air-cooled probe, giving a material temperature of 600°C throughout a 672 hr exposure. The material loss measurements were performed by utilizing an ultrasonic thickness gauge in combination with scanning electron microscopy analysis. It was found that increasing the chromium content significantly reduced the overall material loss of the FeCrAl model alloys but further accelerated the corrosion attack on the windward side. Simultaneously, the increased chromium content caused embrittlement of the material. Minor additions of silicon drastically reduced the material loss of the FeCrAl model alloys, whereas the sample ring with no silicon present was completely deteriorated. The trends observed in this field study correlated well with what has been observed in previous laboratory studies. A state-of-the-art alloy in the present environment, Inconel 625, was simultaneously exposed and showed similar performance to the silicon-containing FeCrAl model alloys with ≥10 wt% Cr.

KEYWORDS

waste-fired boiler, high temperature corrosion, FeCrAl alloys, chromium, silicon

1 | INTRODUCTION

In today's society renewable resources, emitting smaller amounts of greenhouse gases, are becoming increasingly important. The use of fossil fuels is one of the major problems regarding the emission of greenhouse gases[1] and the substitution to other fuels is crucial to reduce the negative impacts on the environment. Biomass and certain types of waste can be combusted in boilers to generate both electricity and heat. These are both renewable and have a relatively low net emission of CO_2 and are therefore good candidates to act as substitutes for fossil fuels. However, altering the fuel from fossil based to biomass and waste is associated with large practical issues originating from the chemical composition of biomass and waste. Upon combusting these, it results in a highly corrosive flue gas due to the presence of large amounts of water vapour, alkali

This is an open access article under the terms of the Creative Commons Attribution License, which permits use, distribution and reproduction in any medium, provided the original work is properly cited.
© 2019 The Authors. *Materials and Corrosion* WILEY-VCH Verlag GmbH & Co. KGaA, Weinheim

chlorides, and HCl (g). Thus, the boiler equipment exhibits accelerated degradation during combustion of biomass and waste.[2–4] Consequently, this leads to increased frequency and cost of maintenance which results in both economic and environmental problems. The superheaters in the boilers are exposed to an especially corrosive environment due to elevated temperatures in this region. Hence, boiler operators generally decrease the steam temperature to increase the lifetime of the superheaters. However, the electrical efficiency of the combustion process is largely dependent on the steam parameters and is reduced with a decrease in steam temperature. Due to this, a larger amount of fuel is needed to produce the same amount of electricity. Thus, to facilitate the substitution of fossil fuels, the steam parameters have to be increased. A solution for this is to use more corrosion resistant materials.

Stainless steels are commonly used in aggressively corrosive environments. However, due to the presence of high amounts of alkali chlorides and water vapour in biomass- and waste-fired boilers, chromia forming stainless steels do not perform well. This is because of the reactions between chromia and water vapour (chromium evaporation)[5] and alkali chlorides (formation of chromates)[6–8] which results in the breakdown of the protective layer. Alumina forming alloys such as FeCrAl alloys are commonly used at high temperatures (above 900°C) in various different applications and have been shown to exhibit excellent corrosion resistance in oxygen and water vapour-containing environments at up to 1300°C[9–11] due to the formation of α-alumina. The reason behind the high corrosion resistance of α-alumina is its high degree of stoichiometry and the low sensitivity towards water vapour and alkali chlorides.[12,13] At temperatures below 900°C, transient alumina has been shown to form at temperatures as low as 600°C,[14] which may not be as resistant towards water vapour and alkali chlorides as α-alumina. This is because they have been reported to contain small amounts of iron and chromium.[15] One approach to tackle this problem is to preoxidize the FeCrAl alloy above 900°C, before exposure, to preform an α-alumina. This has been done by Isrealsson et al [12] and was shown to increase the corrosion resistance in the presence of KCl. However, a negative aspect of this approach is the sensitivity of the α-alumina towards defects, such as microcracks, which has been shown to cause breakaway oxidation as a result of rapid formation of iron-rich oxide,[12] as restoration of the α-alumina scale is not possible below 900°C. This iron-rich oxide scale has been shown to have similar characteristics for both FeCrAl alloys and other ferritic stainless steels and consists of outward growing iron oxide and inward growing spinel.[16–18] Because the primary protection (thin protective oxides such as chromia and alumina) will be lost at an early stage in the harsh environment of the biomass- and waste-fired boilers, another approach may be to improve the properties of the secondary protection (iron-rich oxide).

It has been shown that altering the composition of FeCrAl alloys significantly improves the secondary protection.[19,20] Addition of silicon to a Fe10Cr4Al alloy resulted in a drastic reduction in oxide growth rate when exposed in a lab environment containing oxygen and water vapour in the presence of KCl.[20] In addition, increasing the chromium content in silicon-containing FeCrAl alloys reduced the oxide thickness when exposed to the same conditions.[19] The mechanisms behind these effects are not fully understood and are currently under investigation in parallel studies. The laboratory investigations are very simplified while the intended applications are very complex. It is therefore of interest to investigate if these effects can also be observed during exposure in a waste-fired boiler.

The aim of this study is to investigate the effect of varying chromium and silicon content in FeCrAl model alloys exposed in a commercial waste-fired boiler. Five different model alloys as well as an Inconel 625 reference sample were exposed at the AffaldPlus plant in the Babcock & Wilcox Vølund boiler for 672 hr on an air-cooled probe at a material temperature of 600°C. The deposit compositions were characterised by ion chromatography (IC), whereas material loss measurements were conducted using an ultrasonic thickness gauge. The oxide microstructure was investigated by scanning electron microscopy (SEM) combined with energy-dispersive X-ray (EDX) analysis.

2 | EXPERIMENTAL PROCEDURE

2.1 | Sample preparation

The compositions of the FeCrAl model alloys used in this study are shown in Table 1. All model alloys contained small amounts of the reactive element Zr. In addition to the model

TABLE 1 Nominal chemical composition of the FeCrAl model alloys

Alloys	Fe	Cr	Al	Si	Minor elements
Fe**5Cr**Al2Si	bal.	5	3	2	
Fe**10Cr**Al**2Si**	bal.	10	3	2	
Fe**15Cr**Al2Si	bal.	15	3	2	C, N, Zr
Fe**20Cr**Al2Si	bal.	20	3	2	
Fe10CrAl**0Si**	bal.	10	3	0	

alloys, a 16Mo3 (Fe bal., 0.01 wt% Cr, 0.3 wt% Mo, 0.5 wt% Mn, 0.3 wt% Si) sample ring overwelded with Inconel 625 (Ni bal., 20-23 wt% Cr, 8-10 wt% Mo, 3.15-4.15 wt% Nb + Ta) was exposed and acted as a reference material.

The FeCrAl model alloys were produced by Kanthal (Hallstahammar, Sweden) by induction heating and casting in a copper mould under an argon protective atmosphere which resulted in cylindrical ingots. To remove surface defects the ingots were machined before being forged at 900°C and pressed into the form of a puck. The pucks were then made into rings by lathe machining.

2.2 | Exposure

The exposures were performed at the AffaldPlus plant in the Babcock & Wilcox Vølund boiler which is a waste-fired grate boiler with a thermal capacity of 27 MW. The exposures were performed over the grate at the new steamboost position during a test of boiler settings giving an environment with high flue gas temperature (about 1,000°C) and relatively high levels of Cl. More information regarding the environment at the steamboost position can be found in.[21,22]

An air-cooled probe with two temperature zones was used for exposure of all investigated materials, see Figure 1. To regulate the temperature, two thermocouples were placed in each temperature zone. The material temperature of each zone was then controlled by a proportional-integral derivate (PID) controller and pressurised air was used as cooling agent to achieve a material temperature of 600 ± 3°C. The probe was designed to be able to hold a total of eight samples, four samples in each temperature zone. Before exposure, the thickness of each sample ring was measured at eight points around the ring using an Olympus 38DL PLUS ultrasonic thickness gauge (Olympus, Japan). Because of uneven thickness, this was not performed for the Inconel 625 overwelded sample ring. Before the corrosion test, a deposit test was performed to analyse the composition of the deposit formed under the corrosion test conditions. For the deposit test, rings made of Sanicro 28 (Sandvik AB, Sandviken, Sweden) were used and were exposed for 2 hr. After removal of the probe, the sample rings were detached along with the deposit and stored in a desiccator. The corrosion test was initiated immediately after the deposit test and lasted for 672 hr. After exposure the sample rings were removed from the probe and stored in a desiccator.

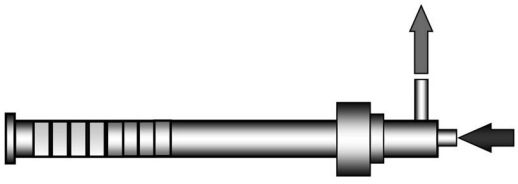

FIGURE 1 Schematic illustration of the air-cooled probe used in this study. The probe can hold up to eight samples at the same time and has two temperature zones (illustrated in yellow and red)

2.3 | Analysis

The composition of the deposit from the 2 hr deposit test was analysed with ion chromatography (IC) using a Dionex ICS-90 system (Thermo Fisher Scientific, Waltham, MA). The anions were analysed with an IonPac AS4A-SC analytic column and 1.8 mM $NaHCO_3$/1.7 mM $NaHCO_3$ was used as solvent. The flow rate was 2 ml/min. A representative and known amount of deposit was removed from the samples and dissolved in 100 ml distilled water. A 5 ml sample of this prepared solution was inserted into the IC column to know the amount of Cl ions and the S/Cl ratio.

The cross sections of the exposed sample rings were prepared by epoxy casting before grinding/polishing. The cast sample rings were ground with SiC paper down to 4000 grit. Before SEM analysis, the cast sample rings were sputtered with a thin gold film to increase the conductivity. The cross sections were analysed by means of SEM (using backscattered electrons [BSE]) and EDX with an accelerating voltage of 20 kV using an FEI Quanta 200 (Thermo Fisher Scientific) equipped with an Oxford Instruments X-Max^N 80T EDX detector (Abingdon, Oxfordshire, England). The thickness of the rings after exposure was measured at eight locations in similar positions as before exposure to evaluate the material loss.

3 | RESULTS

3.1 | Deposit test

Before the exposure a deposit test was performed. The deposit was analysed with ion chromatography to determine the concentration of Cl ions. The amount of deposit collected during the 2 hr deposit test was extrapolated and reached a value of 0.002 $g \cdot mm^{-2} \cdot yr^{-1}$. The concentration of Cl ions was found to be 6.5–8 wt% and the S/Cl ratio was 0.6.

3.2 | Reference material—Inconel 625 overweld

The reference material, 16Mo3 overwelded with Inconel 625, was exposed at the same time and to the same conditions as the other sample rings. No material loss measurements could be performed because of the uneven starting thickness. The SEM/EDX analysis showed that the sample ring had experienced varying degrees of corrosion attack, see Figure 2. On the location of the ring situated towards the windward side, a 300–400 μm thick mixed oxide/deposit layer had formed. The EDX analysis

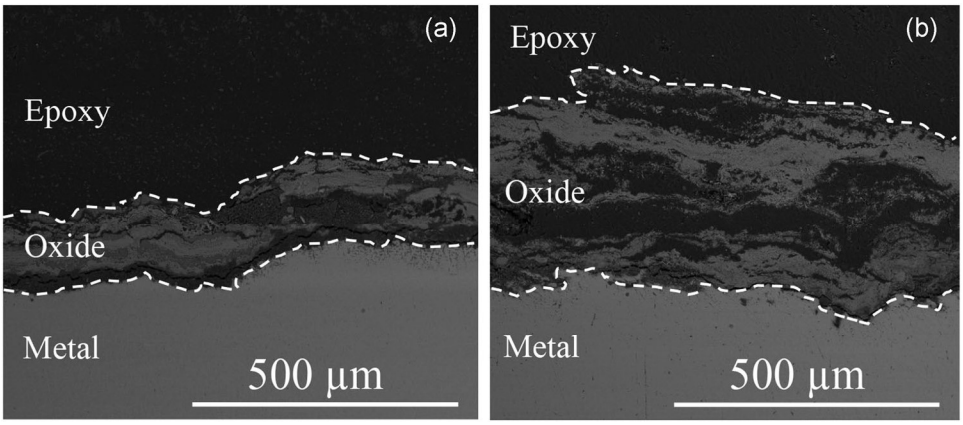

FIGURE 2 SEM-BSE cross section images of the Inconel 625 reference sample after exposure at 600°C for 672 hr at the AffaldPlus plant in the Babcock & Wilcox Vølund boiler. Image (a) shows a location of the ring which exhibited the least corrosion attack. Image (b) shows a location of the ring that was situated on the windward side. BSE: backscattered electrons; SEM: scanning electron microscopy

shows that it mainly consisted of nickel oxide mixed with some remaining deposit species (K, Cl, and S). Minor remains of chromium oxide was observed on the outer part of the nickel oxide. At parts of the ring with indications of lower degree of corrosion attack (left image in Figure 2), a roughly 150 μm thick mixed oxide/deposit layer had formed. It mainly consisted of nickel oxide mixed with significant amounts of deposit species (K, Cl, and S). SEM analysis also detected formation of metal chlorides inside the Inconel 625 layer to a depth of about 80 μm, see Figure 3.

3.3 | FeCrAl model alloys—material loss and microstructure

3.3.1 | Influence of silicon content

Two sample rings with varying silicon content were exposed to examine the effect of minor additions of silicon on the corrosion behaviour. Fe10CrAl**0Si** exhibited a large material loss on the majority of the sample ring, see Figure 4. Three points around the ring displays minor material loss (about 300 μm), whereas the rest of the ring shows severe corrosion attack. At two locations of the ring, situated towards the windward side, no metal remained. A 50–200 μm thick iron-rich oxide was observed with SEM analysis in the areas with minor corrosion attack, see left image of Figure 5. However, at the location situated towards the windward side, the sample ring was corroded through the entire ring, leaving only minor fragments of nonoxidized metal.

Upon adding silicon to the alloy (Fe10CrAl**2Si**), the material loss was largely reduced (displaying a material loss of about 0.25 mm). The SEM analysis of Fe10CrAl**2Si** is presented in Figure 6. In the left image, a 90–160 μm thick oxide was observed and is representative of the majority of the sample ring. The right image shows the location of the ring situated towards the windward side at which a higher degree of corrosion attack had occurred. The corrosion product was up to 400 μm thick and consisted of iron and chromium-rich oxide mixed with large amounts of Cl.

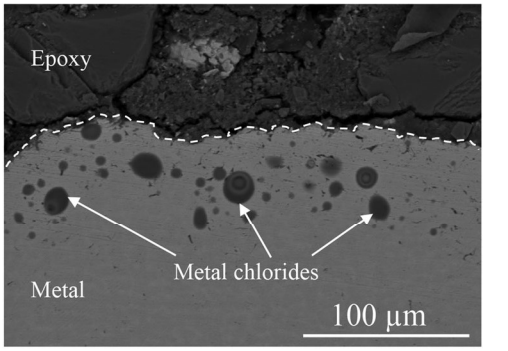

FIGURE 3 SEM-BSE cross section image of the Inconel 625 reference sample after exposure at 600°C for 672 hr at the AffaldPlus plant in the Babcock & Wilcox Vølund boiler. Formation of metal chlorides indicates a highly corrosive environment. BSE: backscattered electrons; SEM: scanning electron microscopy

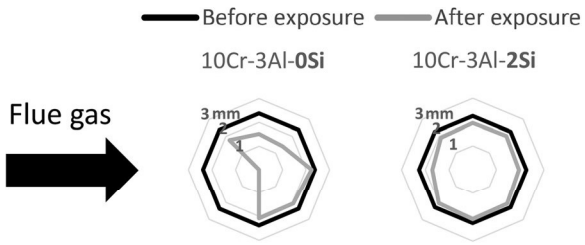

FIGURE 4 Thickness of the sample rings in mm (with varying Si content) at eight points around the rings before and after exposure (672 hr), displaying the material loss for each sample. The windward side is indicated by the arrow

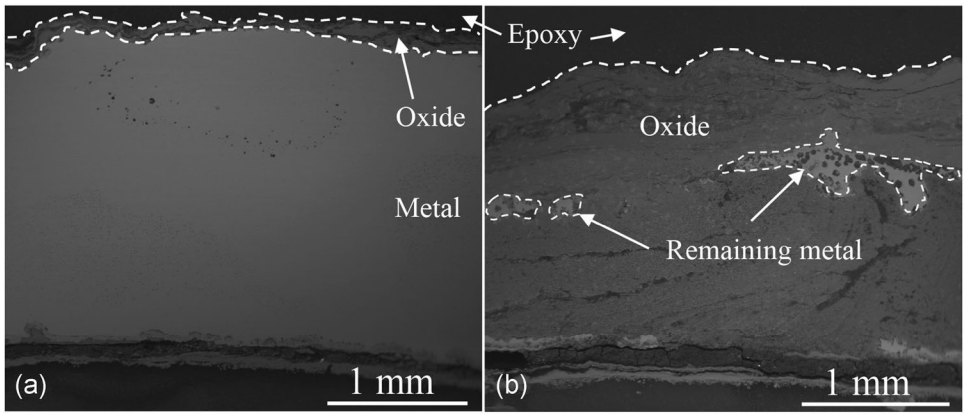

FIGURE 5 SEM-BSE cross section images of Fe10CrAl0Si after exposure at 600°C for 672 hr at the AffaldPlus plant in the Babcock & Wilcox Vølund boiler. Image (a) shows a location of the ring at which minor corrosion attack has taken place. The location of the ring shown in (b) was situated on the windward side. BSE: backscattered electrons; SEM: scanning electron microscopy

3.3.2 | Influence of chromium content

The sample rings with varying chromium content and fixed aluminium and silicon content were exposed to examine the effect of chromium content on the corrosion behaviour. The corrosion attack on the sample rings differed significantly as can be seen in Figure 7. Fe**5Cr**Al2Si has an even material loss of about 0.7 mm around the entire ring. The sample ring exhibits a slightly higher material loss at the location situated towards the windward side (with a material loss of 1 mm). A 0.4–0.6 mm thick oxide could be observed from the SEM analysis (see Figure 8), which, according to EDX analysis, consisted mainly of iron-rich oxide with minor presence of chromium oxide. EDX analysis detected the presence of metal chlorides which were dispersed in the oxide layer.

Fe**10Cr**Al2Si exhibited a significantly lower material loss of about 0.25 mm on the majority of the sample ring (Figure 7). A significant increase in material loss was observed at the location of the ring situated towards the windward side (displaying a material loss of about 0.5 mm). A relatively thin oxide (90–160 μm) could be observed from SEM analysis on the majority of the surface (left image in Figure 6). The oxide mainly consisted of iron-rich oxide with minor presence of chromium and aluminium oxide. On the flue gas side a thicker oxide layer (up to 400 μm) was observed (see right image in Figure 6), which mainly consisted of iron- and chromium-rich oxide mixed with large amounts of Cl (dark contrast areas).

The majority of the Fe**15Cr**Al2Si sample ring displayed negligible material loss, indicating a high corrosion resistance towards the present environments (Figure 7). The location of the ring situated towards the windward side exhibits significantly higher material loss (about 0.5 mm). The majority of the sample ring has formed a very thin and partly detached oxide layer of about 10 μm, see Figure 9 (left image). On the windward side, large oxide formation was observed (right image in Figure 9). The oxide

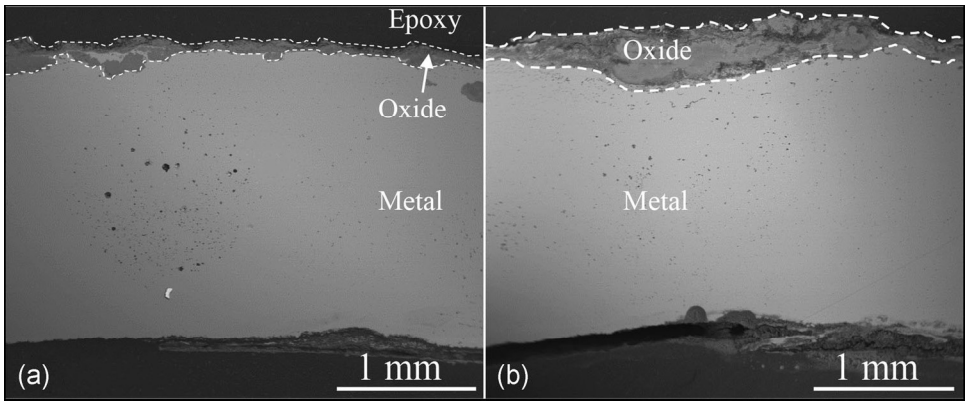

FIGURE 6 SEM-BSE cross section images of Fe10CrAl2Si after exposure at 600°C for 672 hr at the AffaldPlus plant in the Babcock & Wilcox Vølund boiler. Image (a) shows a location of the ring at which minor corrosion attack has taken place. The location of the ring shown in (b) was situated on the windward side. BSE: backscattered electrons; SEM: scanning electron microscopy

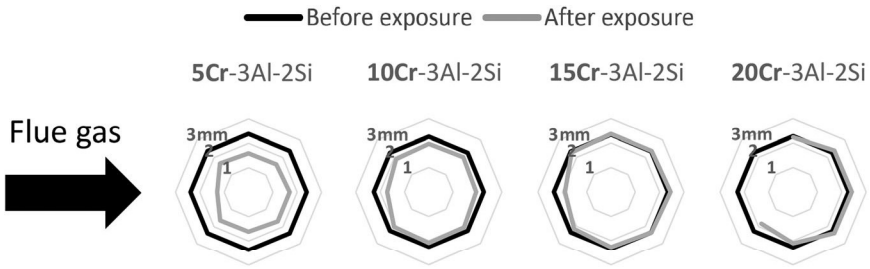

FIGURE 7 Thickness of the sample rings in mm (with varying Cr content) at eight points around the rings before and after exposure (672 hr), displaying the material loss for each sample. The windward side is indicated by the arrow

thickness is undulating, reaching into the sample ring to different depths (ranging from 0.4 to 0.7 mm). EDX analysis showed that it mainly consists of iron- and chromium-rich oxide. A chlorine-rich layer was observed at the metal/oxide interface (distinguished by the darker contrast) which is continuous along the entire corrosion front (see Cl EDX-map in Figure 9).

Fe**20Cr**Al2Si displayed similar behaviour as Fe**15Cr**Al2-Si with only minor material loss on the majority of the sample ring, see Figure 7. However, upon removing the sample ring from the probe it cracked, resulting in the loss of a large part of the ring (hence, the missing measurement points in the circular diagram for Fe**20Cr**Al2Si in Figure 7). SEM analysis showed minor oxide formation on the surface of the sample ring (up to 50 μm thick). Remaining deposit could be observed on a few parts of the sample ring (see left image in Figure 10) with large amounts of Na, K, S, Ca, and Cl. A higher magnification image of the area marked with a square is shown in the right image of Figure 10. A layered structure was observed with deposit on top, followed by outward growing oxide (65–95 μm) and inward growing oxide (roughly 40 μm). Both the inward and outward growing oxides were incorporated with large amounts of Ca and S. Below the oxide layers, a Cl-rich layer (about 50 μm thick with around 20 at% Cl) was detected with large amounts of iron, chromium as well as silicon. According to EDX analysis, the silicon is not evenly distributed in the layer but is concentrated in small particles, spread out within the layer and may be residues from grinding/polishing of the samples.

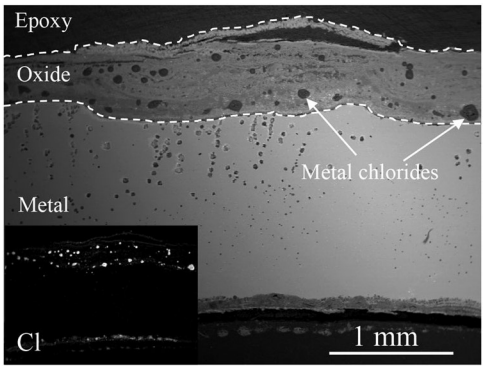

FIGURE 8 SEM-BSE cross section image of Fe5CrAl2Si after exposure at 600°C for 672 hr at the AffaldPlus plant in the Babcock & Wilcox Vølund boiler. BSE: backscattered electrons; SEM: scanning electron microscopy

4 | DISCUSSION

The aim of this study was to investigate the effect of varying chromium content and of minor additions of silicon on the corrosion behaviour of FeCrAl alloys in waste-fired boiler as well as evaluating the potential of utilizing FeCrAl alloys as a superheater material. This has been done by exposing FeCrAl model alloys with varying chromium and silicon content at the AffaldPlus plant in the Babcock & Wilcox Vølund boiler for 672 hr on an air-cooled probe at a material temperature of 600°C.

The exposures were performed at a potential new superheater position in the boiler. The idea behind the steamboost position is to facilitate an increased steam temperature by choosing a superheater position over the grate at which the environment is less corrosive.[21,22] However, during the exposures in this study, the settings were not optimised with regard to Cl^- concentration and temperature (material temperature was regulated but surrounding temperature was very high) giving a very harsh environment and therefore a good test of the new materials.

4.1 | Reference material—Inconel 625 overweld

The reference material used was a 16Mo3 sample ring, overwelded with Inconel 625. This has been exposed various times in similar field exposures (biomass- and waste-fired boilers) due to its exceptionally high corrosion resistance[23–27] and can therefore be used as a measure of the corrosivity of the present conditions. A disadvantage with the overweld is that the sample ring

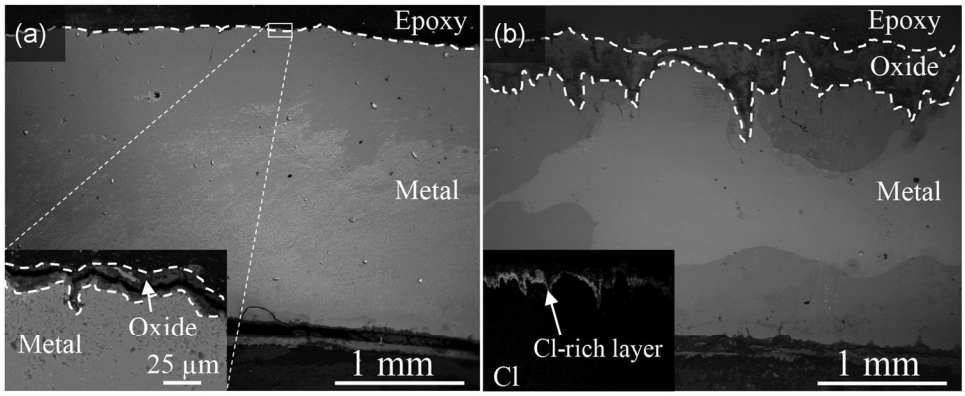

FIGURE 9 SEM-BSE cross section images of Fe15CrAl2Si after exposure at 600°C for 672 hr at the AffaldPlus plant in the Babcock & Wilcox Vølund boiler. Image (a) shows a location of the ring at which only minor corrosion attack has taken place and is representative of the majority of the sample ring. The location of the ring shown in image (b) was situated on the windward side. The darker contrast on the ring in the right image is due to oil covering part of the surface. BSE: backscattered electrons; SEM: scanning electron microscopy

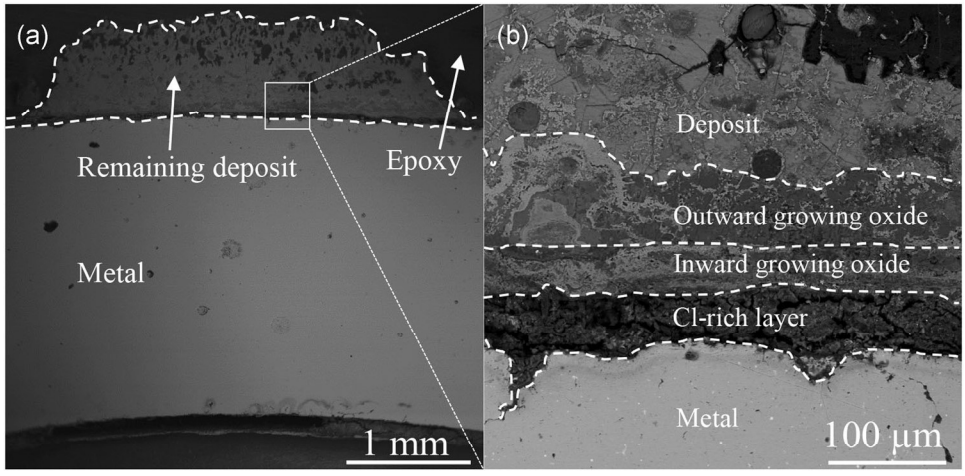

FIGURE 10 SEM-BSE cross section images of Fe20CrAl2Si after exposure at 600°C for 672 hr at the AffaldPlus plant in the Babcock & Wilcox Vølund boiler. Image (a) shows a location of the ring at which deposit remained on the surface. The area marked with the white square is shown in higher magnification in image (b). The dashed lines separates the different oxide layers. BSE: backscattered electrons; SEM: scanning electron microscopy

thickness is not even and accurate thickness measurements for calculation of material loss was therefore not possible. The severity of the corrosion attack on the Inconel 625 overweld is therefore determined by the amount of oxide formation, degree of internal oxidation as well as chlorine penetration (presence of metal chlorides). Possibility of spallation of oxide layers has been taken into consideration when evaluating the extent of the corrosion attack.

An exposure of a 16Mo3 sample ring overwelded with Inconel 625 was previously performed at AffaldPlus plant in the Babcock & Wilcox Vølund boiler at a material temperature of 700°C for 1,000 hr, that is, at slightly higher temperature and for a longer amount of time. SEM analysis of the sample ring showed the formation of

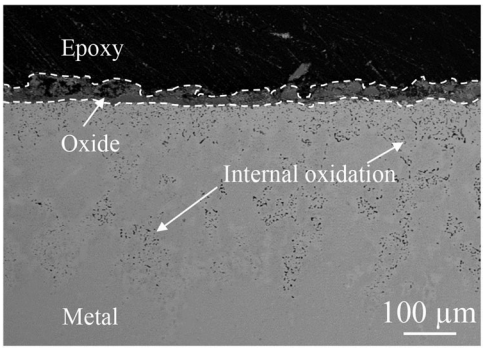

FIGURE 11 SEM-BSE cross section image of the Inconel 625 reference sample after exposure at 700°C for 1,000 hr at the AffaldPlus plant in the Babcock & Wilcox Vølund boiler. BSE: backscattered electrons; SEM: scanning electron microscopy

relatively thin oxide layer (up to 40 μm) as well as internal oxidation to a depth of roughly 350 μm, see Figure 11. However, the Inconel 625 overweld that was exposed in this study exhibits a significantly higher degree of corrosion attack (Figure 2), displaying an average oxide thickness of about 150 μm (300–400 μm on the flue gas side). Taking into consideration that spallation of oxide may occur, these differences in observed oxide thickness does not serve as proof of a more corrosive environment. However, the presence of metal chlorides in the overweld shown in Figure 3 indicates a very high corrosivity as this is rarely observed for Inconel 625. Thus, the environment present during exposure in this study can be considered very corrosive as described above. This should be taken into account when assessing the performance of the FeCrAl model alloys.

4.2 | Effect of silicon addition on the corrosion resistance of FeCrAl model alloys

Minor additions of silicon to alloys has been shown to have positive effects on the corrosion behaviour by reducing the corrosion attack.[20,28–32] The mechanism(s) behind the effect seems to differ depending on alloy composition, temperature, and environment. Upon exposure at elevated temperatures (700°C–900°C) a silicon-containing austenitic stainless steel (353MA) was shown to form a thin SiO_2 layer which may act as a diffusion barrier and prevent further corrosion.[33,34] Increased corrosion resistance and the formation of a SiO_2 layer was also observed for an Fe-20Cr and an Fe-20Cr-20Ni alloy upon addition of silicon in Ar-20CO_2 and Ar-20CO_2-20H_2O at 650°C.[29] In more corrosive environments (in the presence of KCl) modification of Fe-15Cr alloys by addition of aluminium/silicon showed positive synergistic effects on the corrosion behaviour when exposed to air at 650°C.[30,31]

The influence of addition of silicon to FeCrAl alloys was previously studied in differently corrosive environment (O_2, $O_2 + H_2O$, and $O_2 + H_2O + KCl$) at 600°C.[20] Different effects were observed depending on the corrosivity of the environment. In $O_2 + H_2O$, addition of silicon resulted in the prevention of breakaway oxidation caused by evaporation of chromium, indicating that a more aluminium-rich corundum has formed (improving the primary protection). In the presence of KCl, iron-rich oxide formed immediately during exposure. However, silicon addition resulted in a drastic reduction in oxide growth rate (improving the secondary protection).

When exposing similar model FeCrAl alloys in a waste-fired boiler the change of corrosion behaviour upon addition of silicon was in good agreement with the observations in the previously mentioned laboratory study. In the absence of silicon, the FeCrAl alloy severely deteriorated on the majority of the sample and on the windward side (direction of the flue gas) all metal was consumed by the formation iron-rich oxide (see Figure 4 and Figure 5). Addition of silicon to the alloy drastically reduced the material loss of the sample ring, see Figure 6. The majority of the sample ring exhibited relatively thin iron oxide which correlates well with the material loss measurements, indicating that only minor spallation has occurred. Thus, the presence of silicon improved the secondary protection of the alloy by reducing the iron oxide growth rate (secondary protection), which is in good agreement with previous laboratory studies.[20]

4.3 | Effect of chromium content on the corrosion resistance of FeCrAl model alloys

It is well known that chromium is an essential element in stainless steels since it enables them to form a protective chromia layer. Generally, for a steel to be regarded as a stainless steel (with the ability to form chromia) the chromium content needs to exceed 12%. However, in many applications the material is exposed to environments which contain species that react with the chromia and therefore depletes the alloy of chromium. Increasing the chromium content in FeCr alloys has been shown to increase the incubation time before breakaway oxidation (loss of the primary protection) in a water vapour-containing environment at 600°C.[35] However, increasing the chromium content had minor or no effect on the secondary protection (unaltered iron oxide growth rate). Previous studies on FeCrAl model alloys showed that increasing the chromium content significantly reduced the oxide thickness after exposure in an environment containing $O_2 + H_2O$ with KCl present at 600°C.[19] The results indicate that the increased chromium content improves the secondary protection of the alloys.

Accordingly, when exposing similar FeCrAl model alloys in a waste-fired boiler the corrosion behaviour was significantly improved (reduced material loss) upon addition of chromium, see Figure 7. SEM analysis showed that all alloys had formed differently thick iron-rich oxides meaning that they have reached the secondary protection stage. The largest difference in corrosion behaviour is between Fe**5Cr**Al2Si and Fe**10Cr**Al2Si for which the material loss is reduced by roughly 0.5 mm. Increasing the chromium content further results in minor reductions of the overall corrosion attack. This is in good agreement with previous laboratory studies.[19] The location of the material situated towards the flow of the flue gas (windward side)

is known to cause acceleration of the corrosion attack and was observed for all alloys. However, the acceleration of the corrosion attack on the windward side is further pronounced in the alloys with higher chromium content (see right image in Figure 6 and right image in Figure 9). As can be seen the oxide is reaching further into the sample ring of Fe**15Cr**Al2Si compared to Fe**10Cr**Al2Si. Since it is crucial that no part of the material (windward of leeward side) is completely deteriorated, this effect is important to consider when optimising the chromium content. The oxide layers incorporated in the remaining deposit on the surface of Fe**20Cr**Al2Si (right image in Figure 10) indicates that large parts of the oxide layers on the other samples may have spalled off together with the deposit. This may explain the difference in measured material loss and observed oxide thickness (observed oxide thickness is lower than measured material loss).

Apart from improving corrosion behaviour of steels, increasing the chromium content (in combination with relatively high amounts of Si) has also been shown to cause problems regarding mechanical properties (embrittlement) due to the precipitation of a σ phase.[36] High chromium content in combination with aluminium and silicon present in the alloy causes further negative impacts on mechanical properties such as reduced fabricability and embrittlement.[37–39] This is in good agreement with the results from this study as the alloy with the highest amount of chromium (Fe**20Cr**Al2Si) indicated embrittlement as the sample ring cracked during removal from the air-cooled probe. Thus, not only the corrosion properties, affected by the chromium content, has to be considered during optimisation of alloy composition but mechanical properties as well.

4.4 | Comparison of FeCrAl model alloys with state-of-the-art Inconel 625 overweld

As previously mentioned, material loss measurements of the reference sample ring (Inconel 625 overweld) could not be performed as accurately as previous comparisons between the FeCrAl model alloys due to the uneven surface of the overweld. It is therefore difficult to compare the performance of the Inconel 625 overweld with the FeCrAl model alloys. However, it is possible to make a rough estimate of the material loss by assuming that the oxide thickness of the Inconel 625 overweld is equal to the material loss, without taking into consideration that spallation may have occurred. Hence, the minimum material loss (neglecting possible spallation) of the Inconel 625 is compared to the actual material loss of the FeCrAl model alloys. The alloy with silicon absent will not be considered due to severe degradation of the sample ring.

The Inconel 625 overweld displayed varying oxide thicknesses around the sample ring. On the majority of the sample ring, the oxide thickness was around 150 μm, whereas a thicker oxide layer formed on the windward side (300–400 μm), see Figure 2. Fe**5Cr**Al2Si exhibited higher material loss on both the leeward side and windward side (material loss of about 0.7 μm), which is expected with such a low chromium content (in combination with a relatively low aluminium content). Fe**10Cr**Al2Si shows comparable performance to the Inconel 625 overweld, with a material loss of 0.25 mm on the leeward side and 0.5 mm on the windward side. This is promising since the chromium content of this alloy is still relatively low (which reduces the negative interactions of chromium and aluminium on the mechanical properties). Fe**15Cr**Al2Si displays a lower material loss than the Inconel 625 on the leeward side (majority of the sample ring). However, on the windward side, the material loss is higher for Fe**15Cr**Al2Si than for Inconel 625 due to the undulating nature of the corrosion attack for the former (oxide reaching to depths of 0.4–0.7 mm into the metal). The parts of the Fe**20Cr**Al2Si sample ring that remained intact (leeward side) displayed a lower material loss (negligible) than the Inconel 625 sample. However, it is possible that the material loss on the lost part of the sample ring would be larger than the Inconel 625 since it was situated towards the direction of the flue gas (further acceleration of the corrosion attack with higher chromium content observed). Hence, the silicon-containing FeCrAl alloys, except Fe**5Cr**Al2Si, displays similar performance to Inconel 625 in the harsh environment of a waste-fired boiler. Due to negative impacts on mechanical properties (embrittlement and fabricability) and more pronounced acceleration of corrosion attack on the windward side with elevated levels of chromium in the alloy, optimization of the compositions of these type of alloys is needed.

5 | CONCLUSIONS

- Addition of silicon drastically reduced the corrosion attack:
  Large reduction of material loss upon addition of silicon.
  Absence of silicon resulted in total degradation of the majority of the sample ring.
- Large effects on corrosion behaviour upon increasing the chromium content in FeCrAl model alloys:
  Significant overall reduction in material loss.
  Acceleration of corrosion attack on the windward side was further pronounced.

High chromium content alloy indicated alloy embrittlement.

- Silicon-containing FeCrAl alloys with ≥10 wt% chromium indicates comparable corrosion resistance to Inconel 625.

ACKNOWLEDGEMENTS

The work was financed by the Swedish energy agency, administrated by KME, and is part of a collaboration project between Babcock & Wilcox Vølund, Kanthal and the High Temperature Corrosion Center at Chalmers University of Technology.

ORCID

Johan Eklund http://orcid.org/0000-0002-2618-7999

REFERENCES

[1] Union of Concerned Scientists, *Global Warming Effects Around The World. Climate Hot Map*, Union of Concerned Scientists, Cambridge **2011**.
[2] K. O. Davidsson, L.-E. Åmand, B. Leckner, B. Kovacevik, M. Svane, M. Hagström, J. B. C. Pettersson, J. Pettersson, H. Asteman, J.-E. Svensson, L.-G. Johansson, *Energ. Fuels* **2007**, *21*, 71.
[3] H. P. Nielsen, F. J. Frandsen, K. Dam-Johansen, L. L. Baxter, *Prog. Energ. Combust. Sci.* **2000**, *26*, 283.
[4] H. P. Michelsen, F. Frandsen, K. Dam-Johansen, O. H. Larsen, *Fuel Process. Technol.* **1998**, *54*, 95.
[5] H. Asteman, K. Segerdahl, J. E. Svensson, L. G. Johansson, M. Halvarsson, J. E. Tang, in *High Temperature Corrosion and Protection of Materials 6, Prt 1 and 2, Proceedings* P. Steinmetz, I. G. Wright, G. Meier, A. Galerie, B. Pieraggi, R. Podor (Eds:), Trans Tech Publications Ltd, Zurich-Uetikon **2004**, pp. 775–782.
[6] J. Pettersson, N. Folkeson, L.-G. Johansson, J.-E. Svensson, *Oxid. Met.* **2011**, *76*, 93.
[7] C. Pettersson, L. G. Johansson, J. E. Svensson, *Oxid. Met.* **2008**, *70*, 241.
[8] S. Karlsson, J. Pettersson, L. G. Johansson, J. E. Svensson, *Oxid Met* **2012**, *78*, 83.
[9] P. Kofstad, *High temperature corrosion*, Elsevier Applied Science, London; New York, N.Y. **1988**.
[10] H. Götlind, F. Liu, J. E. Svensson, M. Halvarsson, L. G. Johansson, *Oxid Met* **2007**, *67*, 251.
[11] F. Liu, H. Josefsson, J.-E. Svensson, L.-G. Johansson, M. Halvarsson, *Mater. High Temp.* **2005**, *22*, 521.
[12] N. Israelsson, *High Temperature Oxidation and Chlorination of FeCrAl alloys*, Chalmers University of Technology, Gothenburg **2014**.
[13] E. J. Opila, N. S. Jacobson, D. L. Myers, E. H. Copland, *J. Min. Met. Mat. S.* **2006**, *58*, 22.
[14] N. Israelsson, K. Hellström, J.-E. Svensson, L.-G. Johansson, *Oxid. Met.* **2015**, *83*, 1.
[15] H. Josefsson, F. Liu, J. E. Svensson, M. Halvarsson, L. G. Johansson, *Mater. Corros.* **2005**, *56*, 801.
[16] T. Jonsson, H. Larsson, S. Karlsson, H. Hooshyar, M. Sattari, J. Liske, J. E. Svensson, L. G. Johansson, *Oxid. Met.* **2017**, *87*, 333.
[17] T. Jonsson, S. Karlsson, H. Hooshyar, M. Sattari, J. Liske, J. E. Svensson, L. G. Johansson, *Oxid. Met.* **2016**, *85*, 509.
[18] N. Israelsson, K. A. Unocic, K. Hellström, T. Jonsson, M. Norell, J.-E. Svensson, L.-G. Johansson, *Oxid. Met.* **2015**, *84*, 105.
[19] J. Eklund, B. Jönsson, J. Liske, J.-E. Svensson, T. Jonsson, unpublished.
[20] J. Eklund, B. Jönsson, A. Persdotter, J. Liske, J. Svensson, T. Jonsson, *Corrosion Science* **2018**, *144*, 266.
[21] M. D. Paz, J. Phother, T. Jonsson, L. Mikkelsen, Increased steam temperature with Steamboost superheater - The effect of the combustion in deposits and high temperature corrosion, Nordic Flame Days 2017, Stockholm, 2017.
[22] M. D. Paz, Increased steam temperature with Steamboost superheater in grate-fired boilers - Linking deposit formation and high temperature corrosion, Impacts of Fuel Quality on Power Production, Prague, 2016.
[23] M. Montgomery, O. Biede, O. H. Larsen, *Materials Science Forum*, Trans Tech Publ, Zurich **2006**, 523–530.
[24] M. Montgomery, A. Hansson, S. Jensen, T. Vilhelmsen, N. Nielsen, *Mater. Corros.* **2013**, *64*, 14.
[25] M. Montgomery, O. H. Larsen, *Corrosion 2005*, NACE International, Houston **2005**.
[26] N. Henriksen, M. Montgomery, O. H. Larsen, *VDI Bericht* **2002**, *1*, 111.
[27] Y. Alipour, P. Henderson, P. Szakálos, *Mater. Corros.* **2014**, *65*, 217.
[28] Y. Wouters, G. Bamba, A. Galerie, M. Mermoux, J.-P. Petit, *Mater. Sci. Forum* **2004**, *461-464*, 839.
[29] T. D. Nguyen, J. Zhang, D. J. Young, *Oxid. Met.* **2017**, *87*, 541.
[30] Y. S. Li, Y. Niu, M. Spiegel, *Corros. Sci.* **2007**, *49*, 1799.
[31] Y. S. Li, M. Spiegel, S. Shimada, *Mater. Lett.* **2004**, *58*, 3787.
[32] H.-H Mao, X. Qi, J. Cao, L.-C An, Y.-T Yang, *J. Iron Steel Res. Int.* **2017**, *24*, 561.
[33] T. Jonsson, S. Canovic, F. Liu, H. Asteman, J. E. Svensson, L. G. Johansson, M. Halvarsson, *Mater. High Temp.* **2005**, *22*, 231.
[34] T. Jonsson, F. Liu, S. Canovic, H. Asteman, J.-E. Svensson, L.-G. Johansson, M. Halvarsson, *J. Electrochem. Soc.* **2007**, 154.
[35] B. Pujilaksono, T. Jonsson, H. Heidari, M. Halvarsson, J. E. Svensson, L. G. Johansson, *Oxid. Met.* **2011**, *75*, 183.
[36] C.-C. Hsieh, W. Wu, *ISRN Metall.* **2012**, *2012*, 16.
[37] K. G. Field, M. A. Snead, Y. Yamamoto, K. A. Terrani, *Handbook on the Material Properties of FeCrAl Alloys for Nuclear Power Production Applications*, U.S. Department of Energy, Office of Scientific and Technical Information, Oak Ridge **2017**.
[38] S. Chen, L. Rong, *J. Nucl. Mater.* **2015**, *459*, 13.
[39] L. Song, E. Guo, L. Wang, D. Liu, *Metals* **2015**, *5*, 150.

How to cite this article: Eklund J, Paz MD, Jönsson B, Liske J, Svensson JE, Jonsson T. Field exposure of FeCrAl model alloys in a waste-fired boiler at 600°C: The influence of Cr and Si on the corrosion behaviour. *Materials and Corrosion*. 2019;70:1476–1485.
https://doi.org/10.1002/maco.201810618